The effect of random and systematic visual stimulation on entrained infraslow quasi-periodic dynamic global waves in human brain activity

Nan Xu[1], **Derek M. Smith**[2,4], **George Jeno**[3], **Dolly T. Seeburger**[2], **Eric H. Schumacher**[2], **Shella D. Keilholz**[1]

[1]Wallace H. Coulter Department of Biomedical Engineering, Georgia Institute of Technology and Emory University, Atlanta, GA, United States
[2]School of Psychology, Georgia Institute of Technology, Atlanta, GA, United States
[3]School of Computer Science, Georgia Institute of Technology, Atlanta, GA, United States
[4]Department of Neurology, Division of Cognitive Neurology/Neuropsychology,
The Johns Hopkins University School of Medicine, Baltimore, Maryland, United States

Abstract

Infraslow (<0.1Hz) electric activity, involved in attention and arousal fluctuations, serves as the unique neurophysiological basis for infraslow BOLD fluctuations. Particularly, the dynamics of infraslow electrical activity in both resting and task-performing human brains exhibit a quasi-periodic pattern (QPP) of consistent, phase-locked spatiotemporal BOLD signal changes across the whole brain. However, it is unclear how environmental stimuli affect the infraslow dynamic QPP or how the ongoing infraslow dynamics might modify the response to the environment in awake humans. To investigate this, we presented checkerboard sequences flashing at 8Hz to subjects. This is a salient visual stimulus that is known to produce a strong response in visual processing regions. Three central questions were investigated: 1) how does visual stimulation affect the QPPs compared to rest, 2) how does variability in visual stimulus onset affect the QPPs, and 3) how does the BOLD response to visual stimuli depend on the phases of the QPPs. Two different visual stimulation sequences were employed, a systematic stimulation sequence in which the visual stimulus appeared every 20.3 secs and a random stimulation sequence in which the visual stimulus occurred randomly every 14~62.3 secs. Three central observations emerged. First, the two different stimulation sequences affect the QPP waveform in different ways, i.e., the systematic one affecting more on its phase and the random one affecting more on its amplitude. Second, the QPP was more frequent in the systematic condition with significantly shorter intervals between consecutive QPPs compared to the random condition. Third, the BOLD signal response to the visual stimulus across both conditions was swamped by the QPP at the stimulus onset. These results provide novel insights into the relationship between infraslow intrinsic dynamics and task-evoked brain activity.

Introduction

The slow frequency spontaneous fluctuations in blood oxygen level-dependent (BOLD) signals measured by functional magnetic resonance imaging (fMRI) have been a useful measure of brain activity. Because there is a lot of power in the lower frequency range of the BOLD signals (Fox & Raichle, 2007; He & Raichle, 2009), it is important to understand how these low frequency fluctuations in brain activity relate to behavior. The infraslow (less than 0.1Hz) BOLD fluctuations appear to have a unique neurophysiological basis coming from the infraslow neuronal counterpart, i.e., highly correlating with infraslow neuronal activity (Chen et al., 2020; Grooms et al., 2017; Majeed et al., 2009, 2011; Mitra et al., 2018; Pan et al., 2013; Thompson et al., 2014). Such infraslow BOLD-neurophysiological correlate is different and independent from the BOLD-neurophysiological correlates in any of the higher frequency bands (Majeed et al., 2009; Mitra et al., 2018; Pan et al., 2013; Thompson et al., 2013). The infraslow BOLD fluctuations have been found to relate to the large-scale functional architecture of the brain (Biswal et al., 1995). They may also indicate different brain states such as sleep, coma and wakefulness (Lecci et al., 2017; Mitra et al., 2015).

The interactions between the infraslow activity and task- or stimulation-evoked brain responses have been the focus of much research over the last decade. Several studies (Chen et al., 2020; Fox et al., 2005; He, 2013; Huang et al., 2017) reveal that stimulation-evoked BOLD responses are affected by the amplitude of the spontaneous BOLD fluctuations at stimulus onsets, namely, *the prestimulus baseline*, which causes the widely observed *intra*-subject trial-to-trial variability in BOLD responses. In particular, one influential fMRI study suggested that the observed BOLD response is a linear combination of the stimulated response and the prestimulus baseline (Fox et al., 2005). Yet, later works (Chen et al., 2020; He, 2013; Huang et al., 2017) suggest a nonadditive

but inverse modulation between the stimulation and the prestimulus baseline. Specifically, a higher (lower) pre-stimulus baseline results in less (more) activation across widespread brain regions (He, 2013; Huang et al., 2017), and detailed phase-dependent excitation models were revealed in both human (Huang et al., 2017) and rodent brains (Chen et al., 2020).

In these fMRI studies, even though the BOLD responses in the temporally filtered infraslow frequency range (Huang et al., 2017) or the broader low frequency range (Fox et al., 2005; He, 2013) were studied, their underlying neurophysiological correlates remain to be investigated. A pioneering study (Chen et al., 2020) used concurrent calcium and hemodynamic imaging in the somatosensory cortical area of anesthetized rats and found a correlation between the evoked infraslow hemodynamic response and the evoked infraslow neuronal activity. However, Chen and colleagues also found that the infraslow hemodynamic power occurred before the neuronal dynamic power (Chen et al., 2020, Fig. 3ef), which implies that a significant portion of the hemodynamics may not arise from the neuronal level. In summary, the interaction between stimulation and BOLD stimulus responses that arises from the infraslow neuronal activity remains an open question. This question is the focus of the current study.

Previous results demonstrate that the infraslow electric activity is involved in attention (Helps et al., 2010; Monto et al., 2008) and arousal (Raut et al., 2021; Sihn & Kim, 2022). The dynamics of infraslow electric activity in both resting and task-evoked human brains exhibit a quasi-periodic pattern (QPP) of consistent, phase-locked spatiotemporal structure in spontaneous BOLD fluctuations (Abbas, Belloy, et al., 2019; Grooms et al., 2017; Raut et al., 2021; Thompson et al., 2014). More specifically, QPPs consist of a reproducible pattern of spatial changes with a temporal duration of around ~20 seconds that repeat over time, exhibiting alternation of high and low

activity in particular areas and propagation of activity along the cortex. QPPs have been found to represent a different type of dynamics than the higher frequency electrical activity (>0.1Hz) that is tied to the time-varying BOLD correlation (Keilholz et al., 2016; Thompson et al., 2015) or co-activation patterns (X. Zhang et al., 2020) between brain regions. Thus, by investigating stimulus-evoked QPPs, one can indirectly infer the interaction between the stimulation-evoked BOLD response and the spontaneous infraslow neuronal activity.

QPPs display prominent anticorrelation between the default mode network (DMN) and task-positive network (TPN) across rodents and humans (Belloy, Naeyaert, et al., 2018; Majeed et al., 2011; Raut et al., 2021; Yousefi et al., 2018; Yousefi & Keilholz, 2021). It has been shown to be affected by sustained attention and other attention control/working memory tasks (Abbas, Bassil, et al., 2019; Abbas, Belloy, et al., 2019). Recently, it has also been shown to regulate arousal fluctuations (Raut et al., 2021) and modulate sensory responses (Belloy et al., 2021). In particular, a recent study using anesthetized mice suggested that QPPs can be triggered by visual stimulation and that QPPs with different phases prior to the sensory visual stimulus affect the amplitude of the subsequent visual response (Belloy et al., 2021). Despite this progress, more remains to be investigated. Specifically, it is still unclear how environmental perturbations affect the ongoing QPPs and how ongoing QPPs modulate the BOLD responses to these environmental perturbations in humans.

Expanding upon previous findings, here we describe a comprehensive investigation into the relationship between QPPs and visual stimulation in humans. Two conditions of different sequences of visual stimulation induced by flickering checkerboard flashing at 8Hz were employed. One condition involved a systematic stimulation sequence in which the visual stimulus appeared

every 20 secs and the other involved a random stimulation sequence in which has visual stimulus occurred randomly between 14~62.3 secs (average 19.95s+/- 6.37s). Notably, a systematic sequence has been routinely employed for evoking the infraslow spontaneous BOLD signals in the previous studies (Belloy et al., 2021; Duann et al., 2002). These patterns have been shown to entrain the intrinsic rhythms of low frequency brain oscillation to the structure of the attended stimulus stream (Ding et al., 2006; Lakatos et al., 2008) and attract attention in time (Ding et al., 2006; Jones et al., 2002; Lakatos et al., 2008). Additionally, it is worth noting that arousal, which is another factor that associates with QPPs (Raut et al., 2021), is less likely to be much affected by the checkerboard stimulations employed in our study. Yet, there might still be a small increased level of arousal due to uncertainties (Critchley et al., 2001; Ramsøy et al., 2012; Urai et al., 2017; Zhao et al., 2019), specifically the uncertain random stimulus intervals in our context, which is not the main focus of this study.

Because the typical duration of QPPs is ~20 sec in both resting and task-evoked human brains (Abbas, Belloy, et al., 2019; Majeed et al., 2011; Thompson et al., 2014; Yousefi et al., 2018), the predetermined stimulation intervals warrant at most one QPP occurring on or after each stimulus. Thus, we can investigate the one-on-one interaction between an ongoing QPP and the stimulus prior to or overlapping it. Using the resting state results as the control, we specifically attempted to answer the following three questions, 1) how do the QPPs contrast in the two visual conditions, *systematic visual stimulation* and *random visual stimulation*; 2) how do the different sequences of visual stimulation affect the frequency and/or the intervals of consecutive QPPs; and 3) how do different QPP phases prior to the stimulus modulate the subsequent visually evoked BOLD responses for different visual stimulations.

Methods

2.1. Data acquisition and preprocessing

Functional MRI brain images of fourteen young adults (8 women, 6 men) at Atlanta area participated in this experiment (mean age= 19.8$\pm$1.7 yro; range [18-24 yro]). The fMRI scanning was performed at the Center for Advanced Brain Imaging (CABI) at Atlanta on a 3T Seimens Trio scanner with a 12-channel radio frequency coil. For each subject, 7 complete EPI scans were acquired followed by an anatomical scan of T1 image. The anatomical T1 imaging has TE=3.98ms, flip angle=9°, Matrix 256×256 (RO×PE), Slice thickness=1.0 mm with 176 slices and voxel size 1×1×1mm^3. Each EPI scan has 870 time samples, i.e., $N_x = 870$ with the sampling rate, $TR = 0.7$s. Because of the relatively short TRs, the EPI imaging covered the majority of the subcortical and cortical areas with the exceptions of the orbital frontal cortex and temporal pole. Other acquisition parameters of EPI scans include TE=30ms, flip angle=90°, Matrix 64×64 (RO×PE), Slice thickness=3.0mm with 22 slices and voxel size 3.4375×3.4375×3mm^3, Multiband factor=2, Echo spacing= 0.51ms, and BW= 30.637Hz/Px.

Each of the seven EPI scans for each subject fell into one of three distinct experimental conditions. For all subjects, a resting state scan lasting 10.15 minutes (870TRs) was the first functional scan collected. During the resting state scan subjects were told to stay awake and remain still while staring at a fixation cross. After the completion of the resting state scan, six visual stimulation EPI scans were collected. There were two visual stimulation conditions. During both conditions subjects were told to focus on a red fixation cross at the center of the projection screen and that on occasion a flashing checkerboard would appear in the background. For both conditions, the flashing periods were comprised of a black and white checkerboard pattern that inverted every 5

refresh frames (60Hz) for a period of 2.1s (3TRs). The red fixation cross remained at the center of the screen during the checkerboard periods. Half of the scans used a *systematic stimulation* sequence. That is, a flashing checkerboard stimulus appeared for 2.1s (3TRs) every 20.3s (29TRs). The other three scans used a *random stimulation* sequence. That is, the flashing checkerboard stimulus appeared randomly at every 14s~62.3s (20~89TRs, average arrival time 19.95s+/- 6.37s or 28.5+/-9.1TRs). The range of stimulation intervals was selected to warrant that at most one QPP occurs on or after each stimulation onset. For the systematic condition, it also avoids multiple subsequent stimuli overlapping the same ongoing QPP. This allows us to investigate the one-on-one interaction between each ongoing QPP and a stimulus prior to or overlapping it. The two types of stimulation sequences alternated in an ABABAB order, with the order counterbalanced between subjects. An illustrative example of these two different visual stimulation sequences is provided in Fig. S1.

The acquired fMRI data was preprocessed by an automated pipeline based around SPM12 (https://www.fil.ion.ucl.ac.uk/spm/software/spm12/), FSL (Jenkinson et al., 2012), and AFNI (Cox, 1996; Cox & Hyde, 1997). First, the anatomical T1 image was spatially normalized to the 2 mm Montreal Neurological Institute (MNI) atlas. This step includes an image reorientation to the MNI space using FSL, a bias-field correction using FEAT (Y. Zhang et al., 2001), and the SPM segmentation model, which performed the tissue segmentation of grey matter, white matter, cerebrospinal fluid (CSF), bone, soft tissue and air/background of gray matter, and the spatial normalization of these segmented tissues. The binary mask of the white matter, CSF, and the whole brain (gray matter, white matter, and CSF) were obtained by thresholding at the top 70% of these normalized tissues.

Next, the functional EPI timeseries was preprocessed. In order to normalize all scans of each subject to the same template, all seven EPI scans of each subject were first concatenated. Second, the concatenated EPI data was reoriented (FSL), realigned (SPM12), and normalized to the MNI atlas based on the estimates of the SPM segmentation model from the anatomical data preprocessing. In parallel, the motion parameters for the concatenated EPI data, including the framewise displacement (FD) and translation estimates, were also estimated using MCFLIRT (FSL). Third, the normalized EPI data was spatially smoothed with a Gaussian kernel of 4 mm (SPM smooth), and temporally filtered at a bandwidth of 0.01Hz~0.1Hz (AFNI 3dBandpass). Fourth, the EPI data were further regressed by the white matter and CSF signals. Fifth, the concatenated EPI data was split back to each scan. Sixth, for each scan, the motion parameters were examined by the FD as described in (Yousefi et al., 2018). Specifically, scans with mean FD<0.2mm and with a temporal ratio of FD>0.2mm smaller than 40% were included in our analysis (see Fig. S2 for more details) which have proven to robustly detect QPPs (Yousefi et al., 2018).

Finally, the preprocessed EPI timeseries were extracted from the brain parcels provided by the Schaefer-Yeo Atlas (Schaefer et al., 2018) (webpage) and then z-scored. Due to the incomplete brain coverage of the EPI scans, only parcels with over 85% coverage across all subjects were selected from the Schaefer-Yeo Atlas. The percentage of EPI scanning coverage of each Schaefer-Yeo parcel is reported in Fig. S3. Also, because it is well known that visual stimulation will stimulate the visual system, we focused on the BOLD response to the different visual stimulation sequences for regions outside the occipital lobe. In addition, because the temporal lobe was not covered and most of the reminding parcels in the limbic system have less than 85% coverage, the limbic system was also excluded from the analysis. As a result, EPI timeseries from a total of 193

ROIs were extracted, which covered the 5 functional brain networks as described in (Thomas Yeo et al., 2011) including the Somatomotor (SM), Dorsal Attention (DA), Ventral Attention (VA), Frontoparietal (FP) and Default (D) networks. The entire pipeline for preprocessing the partially covered brain fMRI dataset is available on the lab's GitHub Webpage.

In this study, because we are interested in investigating how different visual stimulation (*systematic* or *random*) affects spatiotemporal brain dynamics in comparison with the resting state, the EPI timeseries from each scan were concatenated across all 14 subjects, which results in 1 resting group, 3 repeating groups with systematic stimuli and 3 repeating groups with random stimuli. The three repeating groups with visual stimulations will be used to test the result reproducibility described in later sections. In the remainder of the paper, we refer to this group EPI timeseries as the resting, the systematic 1, 2, or 3, and the random 1, 2, or 3.

2.2. Quasi-periodic pattern detection and examination

The primary QPP is a phase-locked spatiotemporal pattern detected from the BOLD fluctuations, which repeats over time. This dynamic pattern has been found to tie to the infraslow electrical activity (<0.1Hz) (Grooms et al., 2017; Raut et al., 2021; Thompson et al., 2014). In this section, we first describe 1) the detection of the primary QPP and the corresponding QPP with a reverse phase, and then 2) the procedures for comparing different QPPs. 3) Important parameters for detecting and comparing QPPs are included in the final paragraph.

Primary QPP detection. Primary QPP and its occurrence across the entire timeseries for each experimental condition was detected on the group data using the robust QPP detection algorithm described in (Yousefi et al., 2018; Yousefi & Keilholz, 2021). For the resting state condition, the group primary QPP template ($QPPrest$) was obtained by averaging across the segments of EPI

timeseries followed by all supra-threshold peaks (local maxima above a preset positive threshold, described in the last paragraph of this section) of the sliding correlation. These supra-threshold peaks of the sliding correlation value were considered as the ***occurrences of the detected QPP template***, which is further analyzed in the next section. For the systematic condition, timeseries of all 3 repeating groups were concatenated for generating a *group average QPP* template ($QPPsys$) and its occurrence across the concatenated 3 groups. The QPP template for each of these 3 groups (systematic 1, 2, and 3) was also obtained by averaging the EPI segments that follow the correlation local maxima in each group ($\widehat{QPP}sys_i$ for $i = 1,..,3$). Similarly, the group average QPP template ($QPPrand$) and three *group QPPs* ($\widehat{QPP}rand_i$ for $i = 1,..,3$) were obtained for the random stimulation data. Notably, the systematic and random *group average QPPs* have the following relationships: $QPPsys = \sum_{i=1}^{3} \widehat{QPP}sys_i$ and $QPPrand = \sum_{i=1}^{3} \widehat{QPP}rand_i$. We refer to this set of results as *group analytical results*. An illustration of these results and the process that arrived at them are shown in Fig. S5. To further test the reproducibility of the results, we also performed an *independent group analysis*, which detected the QPP independently for each task group, which obtained $QPPsys_i$ and $QPPrand_i$ for $i = 1,..,3$.

Reverse phase QPP detection. Notably, the primary QPP in humans exhibits a sinusoidal waveform (Abbas, Belloy, et al., 2019; Belloy, Shah, et al., 2018; Yousefi et al., 2018; Yousefi & Keilholz, 2021), and the positive QPP and the negative QPP appear to be symmetric in resting state data; moreover, the primary QPP templates may have a reverse phase[1] between randomly selected datasets of resting fMRI (Yousefi et al., 2018; Yousefi & Keilholz, 2021). In our later analysis, we found that the detected primary QPP between different experimental conditions may

[1] If the detected primary QPP starts from positive QPP values which is followed by negative QPP values, then the reverse phase QPP starts from negative QPP values and is followed by positive QPP values, and vice versa.

have a different phase. For the purpose of easy comparison, in addition to the primary QPPs, we also generated the reverse phase QPP template which is corresponding to the primary QPP for each experimental condition, denoted by $QPPrest-$, $QPPsys-$, and $QPPrand-$. Specifically, the reverse phase QPP was obtained by averaging across the segments of EPI timeseries followed by all supra-threshold dips (local minima below a present negative threshold) of the sliding correlation (Yousefi & Keilholz, 2021).

QPP templates comparison. We accessed the distinction of QPP waveforms in the two visual conditions by measuring which drove the QPP to be more different from the reference. For each visual condition, we used the resting QPP which has a similar phase to the stimulated QPP as the null model. The assessment was conducted in the following three steps. First, we measured the correlation coefficients between the stimulated QPP ($QPPsys$ or $QPPrand$) and the resting QPP ($QPPrest$ or $QPPrest-$). Next, to test if the correlation of the two visual conditions is significantly different from each other, a z-test was performed. Specifically, the Fisher z-transformed correlation coefficient was computed from each condition and then the z-score of their differences was computed with sample normalization (Diedenhofen & Musch, 2015). The significance of the difference was also tested at the average level of the three groups (Figs. S6-S7). Then, the distinctions in the entrained QPP waveforms were further examined from the following aspects: 1) the phase shift from the null, 2) the amplitude changes in percentage from the null, 3) the vertical shift in the percentage of the amplitude of the null, and 4) the percentage changes in "peak-life" of the positive and negative peaks from the null (see Fig. 1 (top)). Because the QPP of ROIs in the same brain network was found to share the same waveform (Yousefi et al., 2018; Yousefi & Keilholz, 2021), the waveform examination was conducted at the network level, i.e., the network QPP obtained by averaging the QPP of ROIs in each of the five networks described

in the second to the last paragraph of Section 2.1. More specifically, the phase shift was estimated using (Zhivomirov, 2022) which implements the algorithm in (Sedlacek & Krumpholc, 2005). The "peak-life", in particular, is defined as the entire period that the waveform stays from its peak to half of its peak.

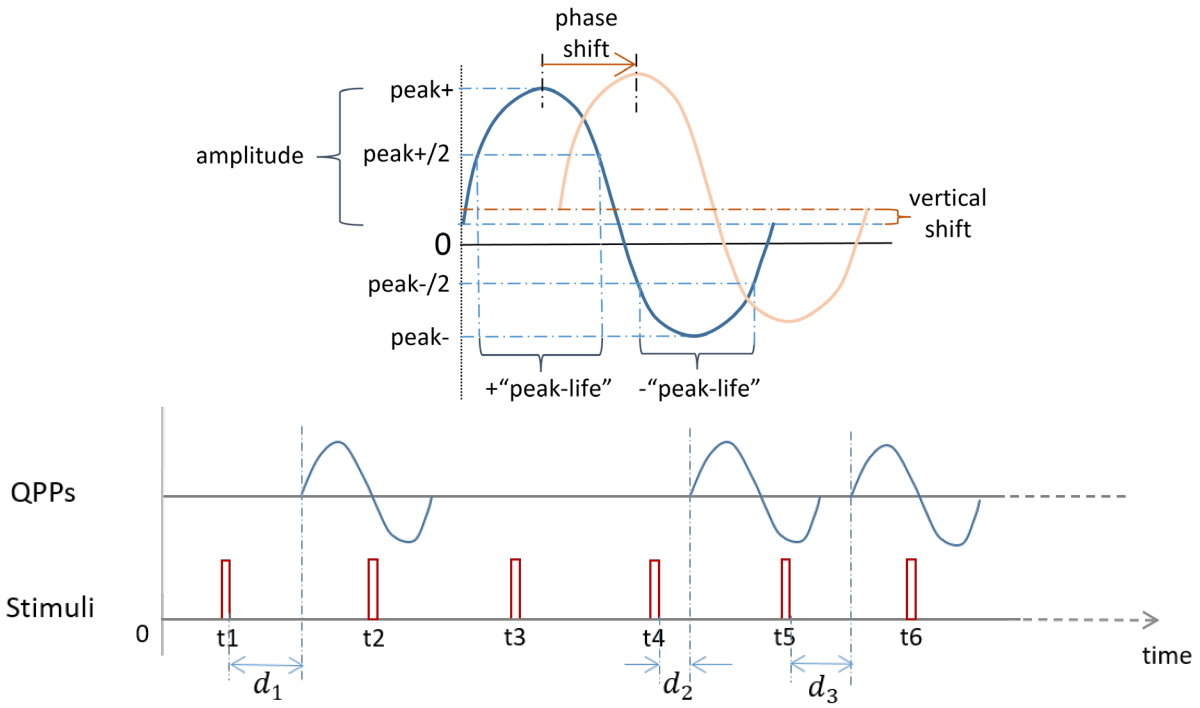

Figure 1 QPP waveform and time delays of QPPs occurrence followed by stimuli. Top: the features which determine a QPP waveform. Bottom: time delay of each ongoing QPP post the stimulus onset, denoted by d_i.

QPP window length and other parameters selection. Because the QPP template lasts for approximately 20s in both resting (Majeed et al., 2011; Thompson et al., 2014; Yousefi et al., 2018) and task-evoked human brains (Abbas, Belloy, et al., 2019), a QPP template duration from 17.5s to 24.5s (PL=25TRs~35TRs) was explored in this study. For the purpose of easy comparison (e.g., for the correlation calculation described in the previous paragraph), one common PL was selected for all three experimental conditions. The final window length PL was determined by when further increasing the PL value will not change the appearance of QPP for all experimental conditions.

Other parameters for detecting the primary QPP include the positive correlation threshold of 0.1 for the first 3 iterations and 0.2 for the rest with a maximum iteration of 20. The negative correlation threshold for detecting the reverse phase QPP was set to be -0.2. The resulting QPP template forms a 2D matrix of 193 ROIs × PL TRs, where PL is the window length.

2.3. Entrained QPP occurrence analysis

We investigated the relationship between the occurrences of QPPs and the onset of visual stimuli. Specifically, two questions were studied, 1) whether different sequences of visual stimulation (i.e., systematic or random) affect the frequency and/or the intervals of consecutive QPPs; and 2) whether the type of visual stimulation sequence affects the onset of successive QPPs.

To answer question 1, the frequency of QPP occurrence across the timecourse for each scan was calculated and compared between the three experimental conditions, which include the time occurrences of $QPPrest$, $QPPsys$ and $QPPrand$. The intervals of consecutive QPPs were also computed, and the mean of the intervals was compared between the two visual conditions. Then, based on the measured mean difference between the two visual conditions, t-test was performed to test if this measured difference is significantly greater or smaller than zero. To investigate question 2, the time delay of QPP occurrence followed by each stimulus was computed for each scan of each subject (Fig. 2 (bottom)). Then, two hypothesis tests were formulated, one for each visual condition. Specifically, the null (and alternative) hypothesis is that the visual stimuli do not (and do) affect (i.e., delay or advance) the QPP. For each visual condition, the null model is that the QPP is the same as the resting state, and therefore, the null distribution can be constructed directly from the resting data. The time delay of QPP occurrence detected from the resting data immediately followed by each visual stimulus was calculated. Because the two types of stimulation

sequences have different onset times (i.e., 29 TRs for systematic stimuli and 20~89 TRs for random stimuli), the time delays of QPP have a different cutoff value for each experimental condition (i.e., <29TRs for the systematic condition and <89TRs for the random condition). Therefore, separate null distribution was generated for each type of stimulus. For each hypothesis test, a two-sample t-test was performed to test if the mean of the empirical result significantly differs from the null model.

2.4. QPP phase-dependent BOLD stimulus response analysis

We investigated how QPPs affect the BOLD response to different stimulation sequences from the following two aspects. First, we examined the distinction in the BOLD stimulated responses between two visual conditions. We focused on the peak value of each stimulus response, which was measured by summing over 4.2s~8.4s (6TR~12TR, totally 7 timepoints) post to a stimulus, and then subtracting the BOLD amplitude at the last timepoint prior to the stimulus for all 7 timepoints (Fig. 3, upper left). This measurement is similar to the calculation described in (He, 2013; Huang et al., 2017), and is due to the fact that the hemodynamic response peaks about 6s post the stimulation onset and has a bandwidth of 4s (Wald & Polimeni, 2015). Means of systematic and random stimulus response as well as the systematic-random contrast were computed across the entire stimulation sequence. ROIs with the significant systematic-random contrast were identified by p-value<0.05 (equivalently zscore>1.96 of <-1.96) after z-scoring the averaged contrasts among ROIs.

Next, we assessed how the visually evoked BOLD response changed when the stimuli occurred at different phases of QPP. BOLD responses in the time segment of [1TR, 29TR] followed by each visual stimulus were inspected. We determined the ranges for the four QPP phases, particularly,

"+zero", "+peak", "-zero", and "-peak", through the following three steps (Fig. 3, left). First, for each ROI, timepoints of the positive and negative peaks of the QPP wave as well as the midpoint(s) where the wave across zero was detected. Second, four pairs of non-overlapping time intervals (δ_i for $i = 1,2,3,4$), which cover the full window length $[0, PL]$, were determined from the detected timepoints. Third, the "+peak" ("-peak") phase range was determined by stepping away from the positive (negative) peak at the corresponding interval δ_i. Forth, the "+zero" ("-zero") range was the none-overlapping interval(s) including the QPP across zero with a positive (negative) trend. A description of phase ranges determined for an illustrative QPP waveform is provided in Fig. 3 (upper right) and the BOLD stimulus responses overlap different phases of the ongoing QPP is illustrated in Fig. 3 (bottom).

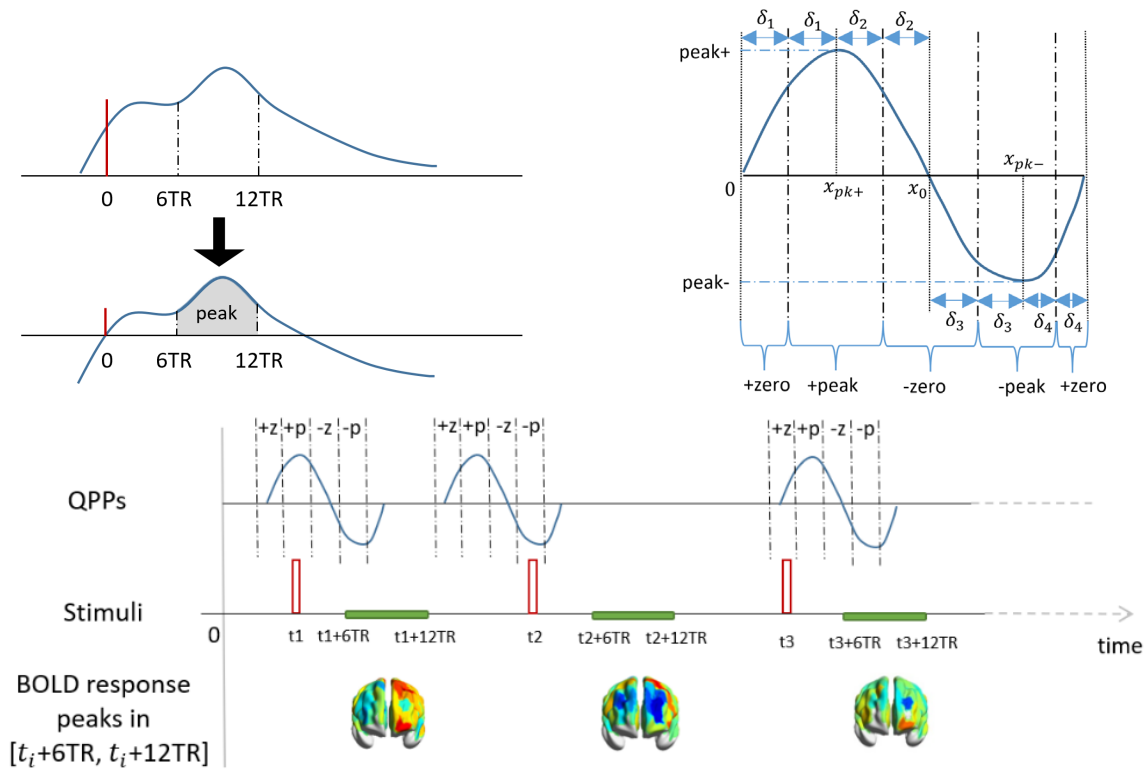

Figure 2 Dependence of the BOLD response to visual stimulation and QPP phase. Upper left: determination of peak value (shaded area) of evoked BOLD responses. The red vertical line depicts the onset of visual stimulation. The BOLD amplitudes in [6TR, 12TR] were subtracted by the BOLD amplitude at the stimulus onset. The gray area under the bottom curve depicts the peak value of the stimulus response. Upper right:

illustration of four phases ranges of a QPP. Let x_{pk+}, x_{pk-}, and x_0 be the timepoint of the positive peak, negative peak, and the midpoint where the QPP wave across the zero, respectively. Based on these timepoints, four pairs of intervals can be determined as $\delta_1 = \frac{x_{pk+}}{2}$, $\delta_2 = \frac{x_0 - x_{pk+}}{2}$, $\delta_3 = \frac{x_{pk-} - x_0}{2}$, and $\delta_4 = \frac{PL - x_{pk-}}{2}$, where PL is the QPP window length. Then, the four phases +zero, +peak, -zero, -peak, have the following ranges $[0, \delta_1] \cup [PL - \delta_4, PL]$, $[x_{pk+} - \delta_1, x_{pk+} + \delta_2]$, $[x_0 - \delta_2, x_0 + \delta_3]$, $[x_{pk-} - \delta_3, x_{pk-} + \delta_4]$. Bottom: BOLD stimulus with stimulus onset overlaps ongoing QPPs at different phases.

Numerically, the whole brain BOLD responses to each stimulus that occurred at each of the four phases of both QPP ($QPPsys$, $QPPrand$) or of its reverse-phase counterpart ($QPPsys-$, $QPPrand-$) were averaged across all stimuli for each phase. The null results (control) were computed by averaging the whole brain BOLD responses to stimuli that have no QPP (including $QPPsys$ and $QPPsys-$ or $QPPrand$ and $QPPrand-$) ongoing. These averaged QPP phase-dependent BOLD responses were compared across ROIs and between the two stimulation sequences as well as between the empirical and null results.

Results

3.1. Distinctions in group average QPPs

Significant differences in group average QPPs for systematic and random visual conditions in comparison to the resting QPP were demonstrated both among all ROIs (Fig. 3 left), and for each network (Fig. 3 right). The group average resting QPP has a significantly lower (z-score=-74.202, p-value<0.01) correlation to $QPPsys$, which is 0.497, compared to the group average $QPPrand$ which has a correlation of 0.906. This significantly lower correlation value also appears in the between-group calculations (Fig. S6, z-score=-75.552, p-value<0.01), as well as in the average of independent groups analysis (Fig. S7, z-score=-13.161, p-value<0.01). Additionally, for the resting state, $QPPrest$ and the $QPPrest-$ were temporally symmetric, which agrees with our previous study (Yousefi et al., 2018; Yousefi & Keilholz, 2021). $QPPsys-$ and $QPPrand-$ are

also shown in Fig. S4. QPPs detected for each independent group are shown in Fig. S7. For each experimental condition, the QPP window length of 21.7s (PL=31TRs) was selected.

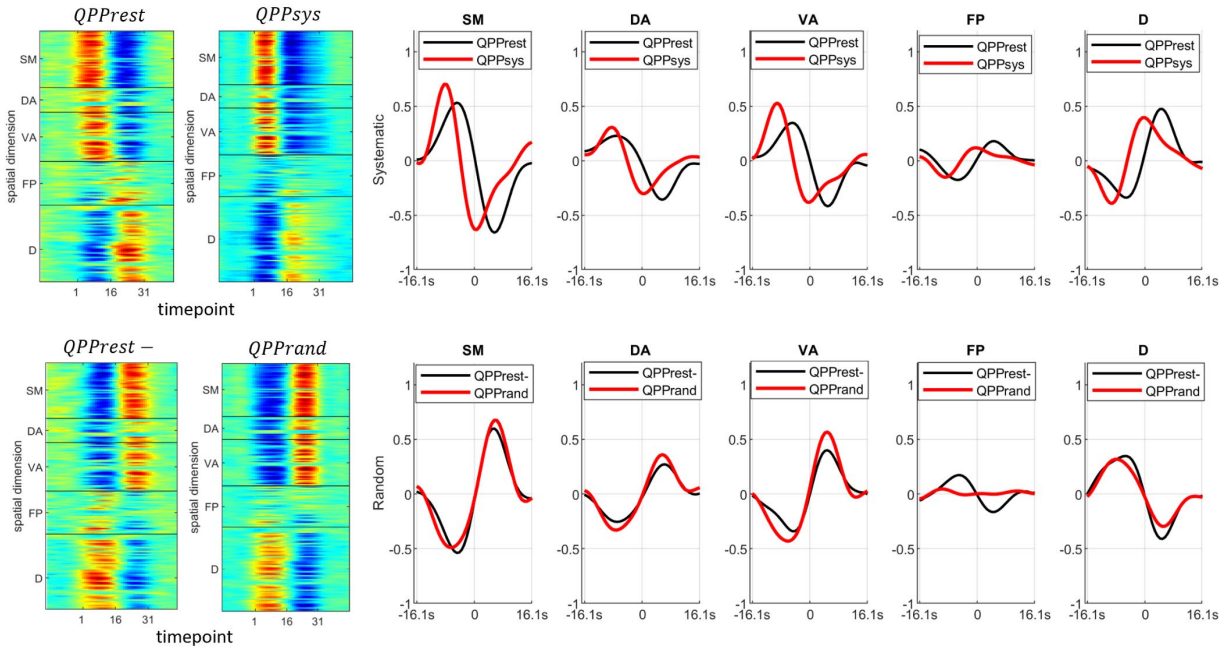

Figure 3 Group average QPP for resting, systematic, and random visual stimuli. Left: the whole brain spatiotemporal pattern across five networks, which include somatomotor (SM), dorsal attention (DA), ventral attention (VA), frontoparietal (FP), and default (D). Right: network QPP averaged among ROIs in each of the five networks. In each plot, the 0s were selected as the timepoint where the magnitude of each network $QPPrest$ or $QPPrest -$ across zero.

		SM	DA	VA	FP	D
Amplitude change (%)	systematic	11.93%	4.03%	18.85%	-23.97%	-3.17%
	random	2.41%	31.14%	34.69%	-72.78%	-19.00%
Phase shift (degree)	systematic	-51.35	-45.42	-50.03	-54.22	-49.20
	random	-4.34	-2.53	-8.46	NA	-1.48
Vertical shift (%)	systematic	4.14%	5.71%	7.08%	-2.50%	-4.09%
	random	2.77%	0.65%	2.58%	-0.61%	2.77%
+ "peak-life" change (%)	systematic	-30.77%	-52.38%	-38.46%	-15.38%	22.22%
	random	0	-9.09%	-10%	-36.36%	-23.53%
– "peak-life" change (%)	systematic	10%	0	70%	-27.27%	-35.71%
	random	25%	-6.67%	15%	NA	22.22%

Table 1 Numerical changes in each network QPP waveform perturbed by the visual stimulation against the resting QPP. Results of the five networks including somatomotor (SM), dorsal attention (DA), ventral attention (VA), frontoparietal (FP), and default (D) are reported, which were computed from the red and black curves in Figure 3 (right). Because the negative phase for the $QPPrand$ for the frontoparietal network is almost zeros, a 'NA' is reported for the phase shift, the peak– change. as well as for the –"peak-life" change.

The values for the effects on network QPP waveforms in the two different visual conditions are tabulated in Table 1. Comparing the systematic and random conditions for each network, several differences are apparent. Specifically, QPP amplitudes increase more in DA and VA and decrease more in FP and D for the random than the systematic condition. Both simulation conditions increase the QPP positively for SM, DA, and VA networks, with the systematic condition elevating more than the random pattern. The phase shift entrained by the systematic stimuli (an average of -50.04 degrees) is greater than the one entrained by the random stimuli (an average of -4.20 degrees). This greater phase shift is also reflected as a squeezed + peak in the task-positive networks for both stimulation sequences. More specifically, the QPP wave's +"peak-life" in DA, VA, and FP networks is shortened by 35.41% on average by the systematic stimuli but only shortened by 18.48% on average by the random stimuli.

3.2. Entrained QPP occurrence

	Group average results	Independent group results
Resting	1.400+/-0.002%	1.400+/-0.002%
Systematic	1.472+/-0.002%	1.541±0.030%
Random	1.396+/-0.002%	1.445±0.046%

Table 2 Frequency of QPP occurrences for each group. For each of the three experimental conditions, the group average result is averaged by the frequency of the group average QPP that occurred in each scan, whereas the independent group result is averaged by the frequency of QPP that is independently detected in each scan.

As shown in Table 2, the frequency of QPP occurrences for the systematic condition is greater than for the random condition, which is similar to the resting state. The mean of QPP intervals for random stimuli is greater than the systematic stimuli no matter on the group average level (i.e., 69.62s for random and 63.46s for systematic) or on the independent group level (see Fig. S9 left). The probability density function of QPP intervals entrained by the two stimulation sequences are compared (Fig. 4a). The mean of the random condition QPP intervals is significantly greater than

the systematic condition (i.e., p-value=0.0004<1% with t-value(881.108)=-3.357 where 881.108 is the degree of freedom). In the independent group analysis, the mean of QPP intervals for the three random groups is significantly greater than for the three systematic groups (see Fig. S9, i.e., t-value(989.233)=-1.875, p-value=0.031<5%).

The probability density function of the time interval between the stimulus and the onset of a subsequent is shown in the violin plot Fig. 4b. These intervals were compared to the null model (computed from the resting data as described in Section 2.3) for each visual stimulation condition. Numerically, despite the slight difference in the mean of QPP delays for the stimulation conditions, neither difference is significant (i.e., the systematic condition has t-value(992.739)=0.879, p-value=0.327>5%, and the random condition has t-value(932.112)=-0.449, p-value=0.327>5%).

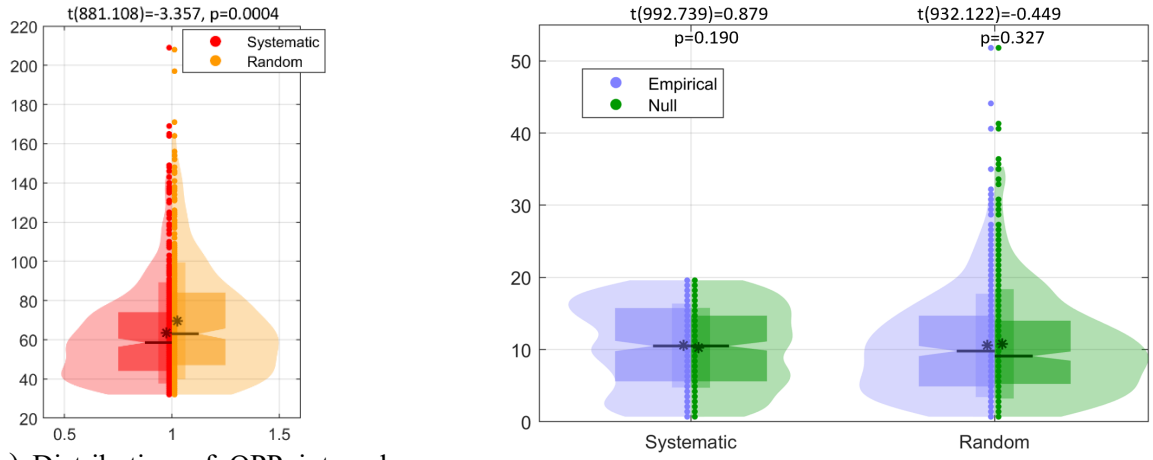

(a) Distribution of QPP intervals for all groups for each visual condition.

(b) Distribution of QPP time delay followed by visual stimuli for all groups in systematic stimulation sequences.

Figure 4 Violin plots of QPP intervals and QPP time delays. For (a), the QPP intervals are contrasted between the two stimulation sequences. For (b), the distribution of QPP time delay in each visual condition is contrasted to its null model. Above each pair of violin distributions, the t-test statistics, t-value(degree of freedom) and p-values are reported. Please see Fig. S9 (right) for the manual description of the violin plot.

3.3. BOLD stimulus response and its QPP phase dependence

The means of the peak value for the BOLD stimulus response for each visual condition, and of the contrast between the two visual conditions are shown in Fig. 5. Four ROIs with significant positive averaged contrast (zscore>1.96) all lie in the bilateral temporoparietal junctions. They have strong positive averaged peak value of BOLD response to systematic stimuli (e.g., at the top 9.64% of all positive mean peak values of BOLD response), and they have strong negative averaged response peak value of random stimuli (e.g., at the bottom 32.2% of all negative mean peak values). On the other hand, the ROI with the significant negative average contrast (zscore<-1.96) is located at the right dorsolateral prefrontal cortex, which has negative averaged peak value of BOLD response to systematic stimuli (i.e., at the bottom 27.27% of all negative mean peak values), and which has strong positive mean peak values to random stimuli (i.e., at the top 6.67% of all positive mean peaks).

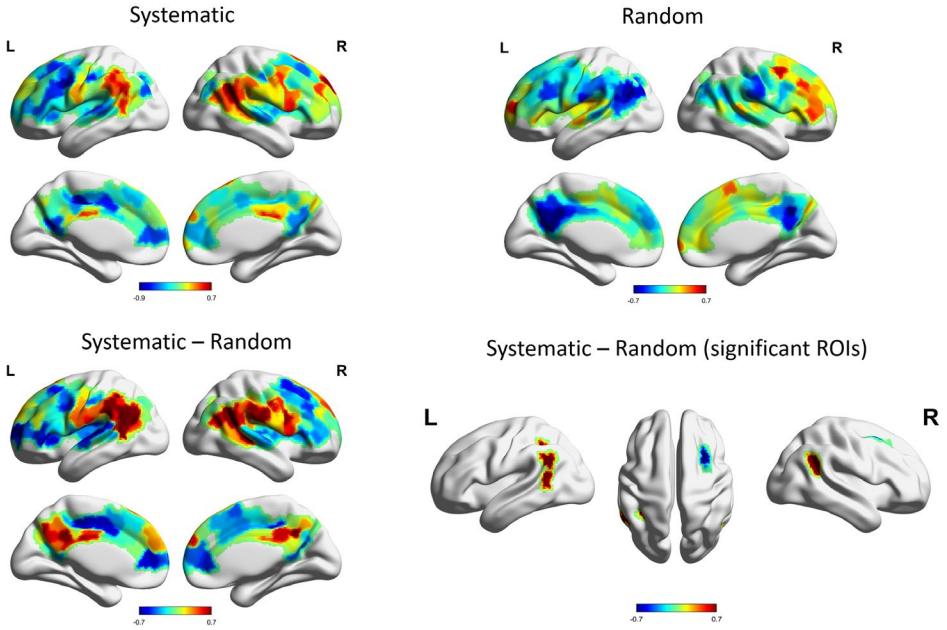

Figure 5 Averaged BOLD responses to systematic and random visual stimulation. Upper: the averaged BOLD response to the systematic (left) and to random (right) stimuli. Bottom: Averaged systematic-random contrast in BOLD stimulus responses (left) and ROIs with absolute zscore>1.96.

The averaged BOLD responses to stimuli that were presented at different phases of QPP for each ROI are organized in the five networks. There are 70.75% of systematic stimuli and 70.61% of random stimuli overlapping with ongoing QPPs. As shown in Fig. 6, for both visual stimulation conditions, the BOLD response to the checkerboard is swamped by the ongoing QPP signals no matter which of the four QPP phases overlap. For example, the stimulation onset in the "+peak" ("-peak") range will follow by a down tread (uprising) BOLD response. In contrast, when the stimulation onset doesn't meet the ongoing QPPs, an average of much moderate BOLD responses appeared, which covers 29.25% or 29.36% of the entire systematic or random stimuli.

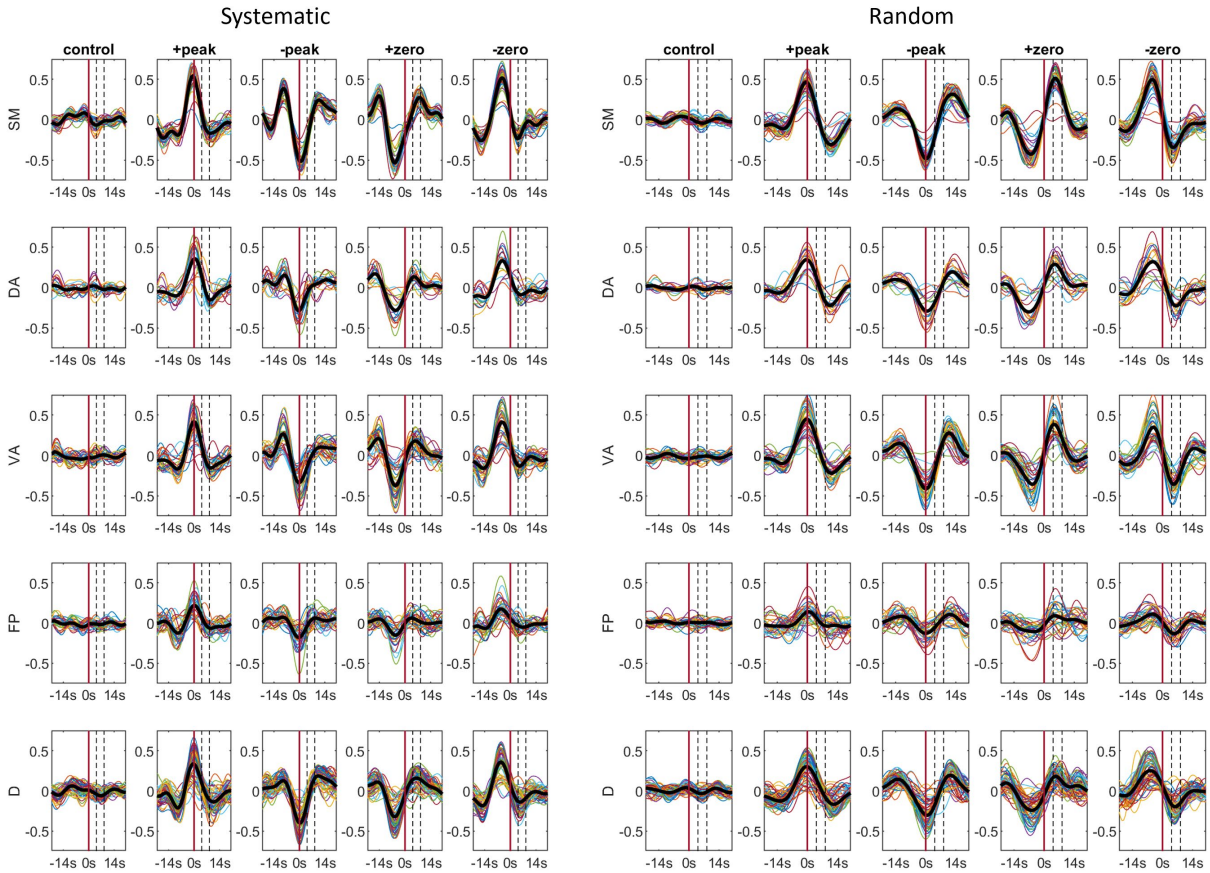

Figure 6 BOLD responses of systematic (left) and random (right) stimulation patterns that are associated with four QPP phases. The vertical axis represents the magnitude of BOLD response whereas the horizontal axis represents the time interval before and after the stimulus onset at 0s, depicted by the red vertical line. The interval between the two dotted vertical lines in each plot depicts the peak range [6TR, 12TR] of the hemodynamic response.

Discussion

The primary QPP is a spatiotemporal pattern detected from the infraslow BOLD fluctuations arising from the infraslow electric activity (Grooms et al., 2017; Raut et al., 2021; Thompson et al., 2014). Thus, the interaction between the ongoing QPPs and visual stimulation relates to the underlying interaction between visual stimulation and the spontaneous infraslow neurophysiological activity. In particular, we investigated how different sequences of visual stimuli affect the primary QPP in awake humans, and how spontaneous QPP prior to each stimulus modifies the subsequent visually evoked BOLD response. Two different types of stimulation sequences were presented alternatively to the subjects, a systematic stimulation sequence in which the visual stimulus appeared every 20.3 secs and a random stimulation sequence which has visual stimulus occurring randomly every 14~62.3 secs. The results of the two types of stimulation sequences were contrasted to the resting state results, which were then compared with each other. Three central observations are discussed below.

Sequences of visual stimulation modify the group averaged QPPs. The QPP entrained by systematic stimulation is significantly different from the one entrained by random stimulation, which looks more like the resting QPP. These differences include a phase modulation and narrowing and increased amplitude of the positive QPP peak in the task-positive network. This is consistent with existing literature in higher frequency activity. For example, the intrinsic (~1.5Hz) delta band oscillation entrained to a systematic stimulus resulted in an increased gain in stimulus response, enforced phase resetting, and enhanced attention performance (Lakatos et al., 2008). Additionally, in a ~7Hz frequency band, the phase of spontaneous oscillations was found to be significantly modulated by only predictable (or attended) but not unpredictable (or unattended) visual stimuli (Busch & VanRullen, 2010). Similarly, in a frequency band of ~8Hz, the phase

coherence was found to be strengthened by a systematic visual attentional task (Zareian et al., 2020).

For the random stimulation condition, our results show effects on the QPP amplitude at a network level. For example, even though the average QPP is amplified in the two attention networks (i.e., DA and VA) due to the visual stimulation, it is much attenuated in FP. The default network QPP is also more attenuated by the random than the systematic stimuli. This type of amplitude changes in infraslow dynamics have also observed in patients with ADHD (Abbas, Bassil, et al., 2019; Helps et al., 2010). This may imply that the attention was distracted in the random visual condition. Specifically, the systematic sequence may entrain intrinsic neural oscillations related to generating expectancies for future events and allocating attention. In contrast, a random presentation of stimuli typically involves a longer reaction time and thus may indicate less sustained attention (e.g., Jones et al., 2002; Lakatos et al., 2008).

Visual stimulation affects both the frequency of QPP occurrence and the BOLD response to the stimulus. Even though the visual conditions have exactly the same number of stimuli, the systematic stimulation produces more frequent QPPs with significantly shorter consecutive QPP intervals than the random stimulation (Fig 4a). However, neither stimulation sequence significantly perturbs the arrival of QPPs. This seems to contradict the previous findings in mice that the primary QPPs are more likely being triggered at the onset of stimulus (Belloy et al., 2021). There are several possible reasons for this discrepancy. First, a very different visual stimulation sequence was employed in (Belloy et al., 2021). Particularly, a stimulation of "ON" (30s) and "OFF" (60s) cycle that repeats over time includes a flickering light constantly flashing at 4 Hz before becoming silence. Second, anesthetized instead of awake mice were studied in (Belloy et

al., 2021), and anesthesia is known to affect infraslow brain dynamics (Pan et al., 2013). Finally, this difference may suggest that the intrinsic QPPs in humans are more robust and less likely to be disrupted by environmental perturbations comparing to anesthetized mice.

In addition, we also found that the two visual stimulation sequences evoked distinct patterns in the BOLD response. For example, bilateral temporoparietal junction was significantly activated by the systematic condition but not the random one (Fig. 5 bottom right). This is consistent with reports that this region is involved in temporal order judgment (Davis et al., 2009) and lack of predictability in the random condition (Wu et al., 2015). On the other hand, the right dorsolateral prefrontal region (around the Brodmann area 9) is strongly activated by random stimulation but not the systematic one (Fig. 5 bottom right). This activation is harder to interpret. This region has been implicated in working memory, planning, and evaluating recency – all processes that may be more active in the random than the systematic condition (Fincham et al., 2002; J. X. Zhang et al., 2003; Zorrilla et al., 1996). However, one should be cautious with these reverse inferences due to the substantial differences between this task and the ones used in previous studies.

The BOLD response is dominated by the QPP waveform when visual stimulation overlaps with ongoing infraslow brain activity. Even though flashing checkerboards are salient visual stimuli known to produce extensive brain activity (Bezdek et al., 2015; Schwartz et al., 2005), across both conditions nearly 70% of the BOLD stimulus responses overlap with and are swamped by ongoing QPP waveforms. The BOLD response in this set is significantly greater than the 30% of trials where the stimulation does not overlap. This observation is distinct from the finding of visually stimulated BOLD response in anesthetized mice (Belloy et al., 2021), which observed the ongoing QPP only moderately affected the amplitude of subsequent stimulus BOLD (Belloy et al., 2021,

Fig. 2D). This result further confirms our conjecture about the robustness of QPP in humans in comparison to mice. In other words, the dynamics of the spontaneous infraslow brain activity in the human brain that supports attention and modulates arousal is highly robust and less likely to be disrupted by environmental perturbations, though the overall dynamic waveform can be perturbed by stimulations in various ways (discussed in the 2nd paragraph in this section).

The widely known trial-to-trial variability in stimulated BOLD responses was popularly examined in a microscopic view in previous studies. A detailed excitation model is often described based on each stimulus and the prestimulus baseline (Chen et al., 2020; Fox et al., 2005; He, 2013; Huang et al., 2017), and inverse modulation between these two factors was observed (Chen et al., 2020; He, 2013; Huang et al., 2017). Complementing these findings, our results explain this trial-to-trial variability from a macroscopic view. In particular, the varying amplitude of BOLD stimulus responses is largely controlled by the intrinsic global fluctuations of QPP – a dynamic pattern that was found arisen from the infraslow neural activity.

Implications for BOLD fMRI. Spontaneous fluctuations in BOLD signals recorded by fMRI link to the underlying neuronal activity through complex neurovascular coupling. Yet, leveraging the multimodal imaging of BOLD and neuronal recordings, various studies reveal BOLD fluctuations directly reflecting the dynamics of neural activity in various frequency bands (Chen et al., 2020; Grooms et al., 2017; Pan et al., 2013; Raut et al., 2021; Thompson et al., 2014, 2015; X. Zhang et al., 2020). In particular, BOLD signals preserve rich information in the infralow frequency range of brain activity. This frequency range was initially dismissed as "noise", artifact, or epi-phenomena in previous studies of circuit-level neural activity (Fox & Raichle, 2007), but has been found to have a unique neurophysiological basis closely linked to attention (Helps et al., 2010; Monto et al., 2008) and arousal (Raut et al., 2021; Sihn & Kim, 2022). More specifically, a quasi-

period dynamic pattern (QPP) detected from the infraslow BOLD fluctuations was found to relate to the infraslow neuronal activity (Chen et al., 2020; Grooms et al., 2017; Pan et al., 2013; Raut et al., 2021; Thompson et al., 2014, 2015; X. Zhang et al., 2020). Thus, investigating QPP allows us to dissect the infraslow neuronal effects in visual stimulus response from the other compounding factors in BOLD signals. This sheds lights on understanding the interaction of environmental perturbation and evoked brain response that directly tie to the neuronal level using this noninvasive imaging technique. In addition, our results reveal that the QPP waveform is not likely to be disrupted but can still be affected by visual stimulation in various ways. This raises the possibility of developing novel non-invasive sensory stimulation procedures to perturb the dynamics of infraslow brain activity to enhance attention in humans.

Acknowledgement

All authors thank National Science Foundation (NSF grant 1533260) for funding support. NX and SDK also thank the funding support from National Institutes of Health (NIH grant R01NS078095). DMS would like to thank the Therapeutic Cognitive Neuroscience Fund. We also thank Dr. Ying Guo for her helpful discussions.

Supplementary Materials

The document of supplementary materials is available at https://www.biorxiv.org/content/10.1101/2022.12.06.519337v2.supplementary-material.

References

Abbas, A., Bassil, Y., & Keilholz, S. (2019). Quasi-periodic patterns of brain activity in individuals with attention-deficit/hyperactivity disorder. *NeuroImage: Clinical*, *21*, 101653. https://doi.org/10.1016/j.nicl.2019.101653

Abbas, A., Belloy, M., Kashyap, A., Billings, J., Nezafati, M., Schumacher, E. H., & Keilholz, S. (2019). Quasi-periodic patterns contribute to functional connectivity in the brain. *NeuroImage*, *191*, 193–204. https://doi.org/10.1016/j.neuroimage.2019.01.076

Belloy, M. E., Billings, J., Abbas, A., Kashyap, A., Pan, W.-J., Hinz, R., Vanreusel, V., van Audekerke, J., van der Linden, A., Keilholz, S. D., Verhoye, M., & Keliris, G. A. (2021). Resting Brain Fluctuations Are Intrinsically Coupled to Visual Response Dynamics. *Cerebral Cortex*, *31*(3), 1511–1522. https://doi.org/10.1093/cercor/bhaa305

Belloy, M. E., Naeyaert, M., Abbas, A., Shah, D., Vanreusel, V., van Audekerke, J., Keilholz, S. D., Keliris, G. A., van der Linden, A., & Verhoye, M. (2018). Dynamic resting state fMRI analysis in mice reveals a set of Quasi-Periodic Patterns and illustrates their relationship with the global signal. In *NeuroImage* (Vol. 180, pp. 463–484). Academic Press Inc. https://doi.org/10.1016/j.neuroimage.2018.01.075

Belloy, M. E., Shah, D., Abbas, A., Kashyap, A., Roßner, S., van der Linden, A., Keilholz, S. D. S. D., Keliris, G. A. G. A., & Verhoye, M. (2018). Quasi-Periodic Patterns of Neural Activity improve Classification of Alzheimer's Disease in Mice. *Scientific Reports*, *8*(1), 10024. https://doi.org/10.1038/s41598-018-28237-9

Bezdek, M. A., Gerrig, R. J., Wenzel, W. G., Shin, J., Pirog Revill, K., & Schumacher, E. H. (2015). Neural evidence that suspense narrows attentional focus. *Neuroscience*, *303*, 338–345. https://doi.org/10.1016/J.NEUROSCIENCE.2015.06.055

Biswal, B., Yetkin, F. Z., Haughton, V. M., & Hyde, J. S. (1995). Functional connectivity in the motor cortex of resting human brain using echo-planar MRI. *Magn Reson Med*, *34*(4), 537–541. https://www.ncbi.nlm.nih.gov/pubmed/8524021

Busch, N. A., & VanRullen, R. (2010). Spontaneous EEG oscillations reveal periodic sampling of visual attention. *Proceedings of the National Academy of Sciences of the United States of America*, *107*(37), 16048–16053. https://doi.org/10.1073/PNAS.1004801107/SUPPL_FILE/PNAS.201004801SI.PDF

Chen, W., Park, K., Pan, Y., Koretsky, A. P., & Du, C. (2020). Interactions between stimuli-evoked cortical activity and spontaneous low frequency oscillations measured with neuronal calcium. *NeuroImage*, *210*, 116554. https://doi.org/10.1016/J.NEUROIMAGE.2020.116554

Cox, R. W. (1996). AFNI: Software for analysis and visualization of functional magnetic resonance neuroimages. *Computers and Biomedical Research*, *29*(3), 162–173. https://doi.org/10.1006/cbmr.1996.0014

Cox, R. W., & Hyde, J. S. (1997). Software tools for analysis and visualization of fMRI data. *NMR in Biomedicine*, *10*(4–5), 171–178. https://doi.org/10.1002/(SICI)1099-1492(199706/08)10:4/5<171::AID-NBM453>3.0.CO;2-L

Critchley, H. D., Mathias, C. J., & Dolan, R. J. (2001). Neural activity in the human brain relating to uncertainty and arousal during anticipation. *Neuron*, *29*(2), 537–545. https://doi.org/10.1016/S0896-6273(01)00225-2

Davis, B., Christie, J., & Rorden, C. (2009). Temporal Order Judgments Activate Temporal Parietal Junction. *The Journal of Neuroscience*, *29*(10), 3182. https://doi.org/10.1523/JNEUROSCI.5793-08.2009

Diedenhofen, B., & Musch, J. (2015). cocor: A Comprehensive Solution for the Statistical Comparison of Correlations. *PLoS ONE*, *10*(4). https://doi.org/10.1371/JOURNAL.PONE.0121945

Ding, J., Sperling, G., & Srinivasan, R. (2006). Attentional Modulation of SSVEP Power Depends on the Network Tagged by the Flicker Frequency. *Cerebral Cortex*, *16*(7), 1016–1029. https://doi.org/10.1093/CERCOR/BHJ044

Duann, J. R., Jung, T. P., Kuo, W. J., Yeh, T. C., Makeig, S., Hsieh, J. C., & Sejnowski, T. J. (2002). Single-Trial Variability in Event-Related BOLD Signals. *NeuroImage*, *15*(4), 823–835. https://doi.org/10.1006/NIMG.2001.1049

Fincham, J. M., Carter, C. S., van Veen, V., Stenger, V. A., & Anderson, J. R. (2002). Neural mechanisms of planning: A computational analysis using event-related fMRI. *Proceedings of the National Academy of Sciences*, *99*(5), 3346–3351. https://doi.org/10.1073/PNAS.052703399

Fox, M. D., & Raichle, M. E. (2007). Spontaneous fluctuations in brain activity observed with functional magnetic resonance imaging. *Nature Reviews Neuroscience 2007 8:9*, *8*(9), 700–711. https://doi.org/10.1038/nrn2201

Fox, M. D., Snyder, A. Z., Zacks, J. M., & Raichle, M. E. (2005). Coherent spontaneous activity accounts for trial-to-trial variability in human evoked brain responses. *Nature Neuroscience 2005 9:1*, *9*(1), 23–25. https://doi.org/10.1038/nn1616

Grooms, J. K., Thompson, G. J., Pan, W. J., Billings, J., Schumacher, E. H., Epstein, C. M., & Keilholz, S. D. (2017). Infraslow Electroencephalographic and Dynamic Resting State Network Activity. *Brain Connectivity*, *7*(5), 265. https://doi.org/10.1089/BRAIN.2017.0492

He, B. J. (2013). Spontaneous and Task-Evoked Brain Activity Negatively Interact. *Journal of Neuroscience*, *33*(11), 4672–4682. https://doi.org/10.1523/JNEUROSCI.2922-12.2013

He, B. J., & Raichle, M. E. (2009). The fMRI signal, slow cortical potential and consciousness. *Trends in Cognitive Sciences*, *13*(7), 302–309. https://doi.org/10.1016/j.tics.2009.04.004

Helps, S. K., Broyd, S. J., James, C. J., Karl, A., Chen, W., & Sonuga-Barke, E. J. S. (2010). Altered spontaneous low frequency brain activity in Attention Deficit/Hyperactivity Disorder. *Brain Research*, *1322*, 134–143. https://doi.org/10.1016/j.brainres.2010.01.057

Huang, Z., Zhang, J., Longtin, A., Dumont, G., Duncan, N. W., Pokorny, J., Qin, P., Dai, R., Ferri, F., Weng, X., & Northoff, G. (2017). Is There a Nonadditive Interaction Between Spontaneous and Evoked Activity? Phase-Dependence and Its Relation to the Temporal Structure of Scale-Free Brain Activity. *Cerebral Cortex*, *27*(2), 1037–1059. https://doi.org/10.1093/CERCOR/BHV288

Jenkinson, M., Beckmann, C. F., Behrens, T. E. J., Woolrich, M. W., & Smith, S. M. (2012). FSL. *NeuroImage*, *62*(2), 782–790. https://doi.org/10.1016/j.neuroimage.2011.09.015

Jones, M. R., Moynihan, H., MacKenzie, N., & Puente, J. (2002). Temporal aspects of stimulus-driven attending in dynamic arrays. *Psychological Science*, *13*(4), 313–319. https://doi.org/10.1111/1467-9280.00458

Keilholz, S. D., Pan, W.-J., Billings, J., Nezafati, M., & Shakil, S. (2016). Noise and non-neuronal contributions to the BOLD signal: applications to and insights from animal studies. *NeuroImage*. https://doi.org/10.1016/j.neuroimage.2016.12.019

Lakatos, P., Karmos, G., Mehta, A. D., Ulbert, I., & Schroeder, C. E. (2008). Entrainment of neuronal oscillations as a mechanism of attentional selection. *Science*, *320*(5872), 110–113. https://doi.org/10.1126/SCIENCE.1154735/SUPPL_FILE/LAKATOS.SOM.PDF

Lecci, S., Fernandez, L. M. J., Weber, F. D., Cardis, R., Chatton, J. Y., Born, J., & Lüthi, A. (2017). Coordinated infraslow neural and cardiac oscillations mark fragility and offline periods in mammalian sleep. *Science Advances*, *3*(2). https://doi.org/10.1126/SCIADV.1602026/SUPPL_FILE/1602026_SM.PDF

Majeed, W., Magnuson, M., Hasenkamp, W., Schwarb, H., Schumacher, E. H. H. E. H. H., Barsalou, L., & Keilholz, S. D. D. S. D. (2011). Spatiotemporal dynamics of low frequency BOLD fluctuations in rats and humans. *Neuroimage*, *54*(2), 1140–1150. https://doi.org/10.1016/j.neuroimage.2010.08.030

Majeed, W., Magnuson, M., Keilholz, S. D. S. D., & Majeed M.; Keilholz, S., W. M. (2009). Spatiotemporal dynamics of low frequency fluctuations in BOLD fMRI of the rat. *J Magn Reson Imag*, *30*(2), 384–393. https://doi.org/10.1002/jmri.21848

Mitra, A., Kraft, A., Wright, P., Acland, B., Snyder, A. Z., Rosenthal, Z., Czerniewski, L., Bauer, A., Snyder, L., Culver, J., Lee, J. M., & Raichle, M. E. (2018). Spontaneous Infra-slow Brain Activity Has Unique Spatiotemporal Dynamics and Laminar Structure. *Neuron*, *98*(2), 297-305.e6. https://doi.org/10.1016/j.neuron.2018.03.015

Mitra, A., Snyder, A. Z., Tagliazucchi, E., Laufs, H., & Raichle, M. E. (2015). Propagated infra-slow intrinsic brain activity reorganizes across wake and slow wave sleep. *ELife*, *4*(NOVEMBER2015). https://doi.org/10.7554/ELIFE.10781.001

Monto, S., Palva, S., Voipio, J., & Palva, J. M. (2008). Very Slow EEG Fluctuations Predict the Dynamics of Stimulus Detection and Oscillation Amplitudes in Humans. *Journal of Neuroscience*, *28*(33), 8268–8272. https://doi.org/10.1523/JNEUROSCI.1910-08.2008

Pan, W.-J., Thompson, G. J., Magnuson, M. E., Jaeger, D., & Keilholz, S. (2013). Infraslow LFP correlates to resting-state fMRI BOLD signals. *Neuroimage*, *74*(0), 288–297. https://doi.org/10.1016/j.neuroimage.2013.02.035

Ramsøy, T. Z., Friis-Olivarius, M., Jacobsen, C., Jensen, S. B., & Skov, M. (2012). Effects of perceptual uncertainty on arousal and preference across different visual domains. *Journal of Neuroscience, Psychology, and Economics*, *5*(4), 212–226. https://doi.org/10.1037/A0030198

Raut, R. v., Snyder, A. Z., Mitra, A., Yellin, D., Fujii, N., Malach, R., & Raichle, M. E. (2021). Global waves synchronize the brain's functional systems with fluctuating arousal. *Science Advances*, *7*(30). https://doi.org/10.1126/SCIADV.ABF2709/SUPPL_FILE/SCIADV.ABF2709_SM.PDF

Schaefer, A., Kong, R., Gordon, E. M., Laumann, T. O., Zuo, X.-N., Holmes, A. J., Eickhoff, S. B., & Yeo, B. T. T. (2018). Local-Global Parcellation of the Human Cerebral Cortex from Intrinsic Functional Connectivity MRI. *Cerebral Cortex*, *28*(9), 3095–3114. https://doi.org/10.1093/cercor/bhx179

Schwartz, S., Vuilleumier, P., Hutton, C., Maravita, A., Dolan, R. J., & Driver, J. (2005). Attentional load and sensory competition in human vision: modulation of fMRI responses by load at fixation during task-irrelevant stimulation in the peripheral visual field. *Cerebral Cortex (New York, N.Y. : 1991)*, *15*(6), 770–786. https://doi.org/10.1093/CERCOR/BHH178

Sedlacek, M., & Krumpholc, M. (2005). Digital measurement of phase difference - a comparative study of DSP algorithms. *Metrology and Measurement Systems*, *Vol. 12*(nr 4), 427–448.

Sihn, D., & Kim, S. P. (2022). Brain Infraslow Activity Correlates With Arousal Levels. *Frontiers in Neuroscience*, *16*, 230. https://doi.org/10.3389/FNINS.2022.765585/BIBTEX

Thomas Yeo, B. T., Krienen, F. M., Sepulcre, J., Sabuncu, M. R., Lashkari, D., Hollinshead, M., Roffman, J. L., Smoller, J. W., Zöllei, L., Polimeni, J. R., Fisch, B., Liu, H., Buckner, R. L., Fischl, B., Liu, H., Buckner, R. L., Yeo, B. T., Krienen, F. M., Sepulcre, J., … Buckner, R. L. (2011). The organization of the human cerebral cortex estimated by intrinsic functional connectivity. *J Neurophysiol*, *106*(3), 1125–1165. https://doi.org/10.1152/jn.00338.2011

Thompson, G. J., Merritt, M. D., Pan, W.-J., Magnuson, M. E., Grooms, J. K., Jaeger, D., & Keilholz, S. D. (2013). Neural correlates of time-varying functional connectivity in the rat. *NeuroImage*, *83*(0), 826–836. https://doi.org/10.1016/j.neuroimage.2013.07.036

Thompson, G. J., Pan, W. J., & Keilholz, S. D. (2015). Different dynamic resting state fMRI patterns are linked to different frequencies of neural activity. *Journal of Neurophysiology*, *114*(1), 114–124. https://doi.org/10.1152/jn.00235.2015

Thompson, G. J., Pan, W. J., Magnuson, M. E., Jaeger, D., & Keilholz, S. D. (2014). Quasi-periodic patterns (QPP): Large-scale dynamics in resting state fMRI that correlate with local infraslow electrical activity. *NeuroImage*, *84*, 1018–1031. https://doi.org/10.1016/j.neuroimage.2013.09.029

Urai, A. E., Braun, A., & Donner, T. H. (2017). Pupil-linked arousal is driven by decision uncertainty and alters serial choice bias. *Nature Communications 2017 8:1*, *8*(1), 1–11. https://doi.org/10.1038/ncomms14637

Wald, L. L., & Polimeni, J. R. (2015). High-Speed, High-Resolution Acquisitions. *Brain Mapping: An Encyclopedic Reference*, *1*, 103–116. https://doi.org/10.1016/B978-0-12-397025-1.00011-7

Wu, Q., Chang, C. F., Xi, S., Huang, I. W., Liu, Z., Juan, C. H., Wu, Y., & Fan, J. (2015). A critical role of temporoparietal junction in the integration of top-down and bottom-up attentional control. *Human Brain Mapping*, *36*(11), 4317–4333. https://doi.org/10.1002/HBM.22919

Yousefi, B., & Keilholz, S. (2021). Propagating patterns of intrinsic activity along macroscale gradients coordinate functional connections across the whole brain. *NeuroImage*, *231*, 117827. https://doi.org/10.1016/j.neuroimage.2021.117827

Yousefi, B., Shin, J., Schumacher, E. H., & Keilholz, S. D. (2018). Quasi-periodic patterns of intrinsic brain activity in individuals and their relationship to global signal. *NeuroImage*, *167*, 297–308. https://doi.org/10.1016/j.neuroimage.2017.11.043

Zareian, B., Maboudi, K., Daliri, M. R., Abrishami Moghaddam, H., Treue, S., & Esghaei, M. (2020). Attention strengthens across-trial pre-stimulus phase coherence in visual cortex, enhancing stimulus processing. *Scientific Reports 2020 10:1*, *10*(1), 1–12. https://doi.org/10.1038/s41598-020-61359-7

Zhang, J. X., Leung, H. C., & Johnson, M. K. (2003). Frontal activations associated with accessing and evaluating information in working memory: An fMRI study. *NeuroImage*, *20*(3), 1531–1539. https://doi.org/10.1016/j.neuroimage.2003.07.016

Zhang, X., Pan, W. J., & Keilholz, S. D. (2020). The relationship between BOLD and neural activity arises from temporally sparse events. *NeuroImage*, *207*, 116390. https://doi.org/10.1016/j.neuroimage.2019.116390

Zhang, Y., Brady, M., & Smith, S. (2001). Segmentation of brain MR images through a hidden Markov random field model and the expectation-maximization algorithm. *IEEE Transactions on Medical Imaging*, *20*(1), 45–57. https://doi.org/10.1109/42.906424

Zhao, S., Chait, M., Dick, F., Dayan, P., Furukawa, S., & Liao, H. I. (2019). Pupil-linked phasic arousal evoked by violation but not emergence of regularity within rapid sound sequences.

Nature Communications 2019 10:1, *10*(1), 1–16. https://doi.org/10.1038/s41467-019-12048-1

Zhivomirov, H. (2022). *Phase Difference Measurement with Matlab*. MATLAB Central File Exchange. https://www.mathworks.com/matlabcentral/fileexchange/48025-phase-difference-measurement-with-matlab

Zorrilla, L. T., Aguirre, G. K., Zarahn, E., Cannon, T. D., & D'Esposito, M. (1996). Activation of the prefrontal cortex during judgments of recency: a functional MRI study. *Neuroreport*, *7*(15–17), 2803–2806. https://doi.org/10.1097/00001756-199611040-00079